Supplementary Figure S1

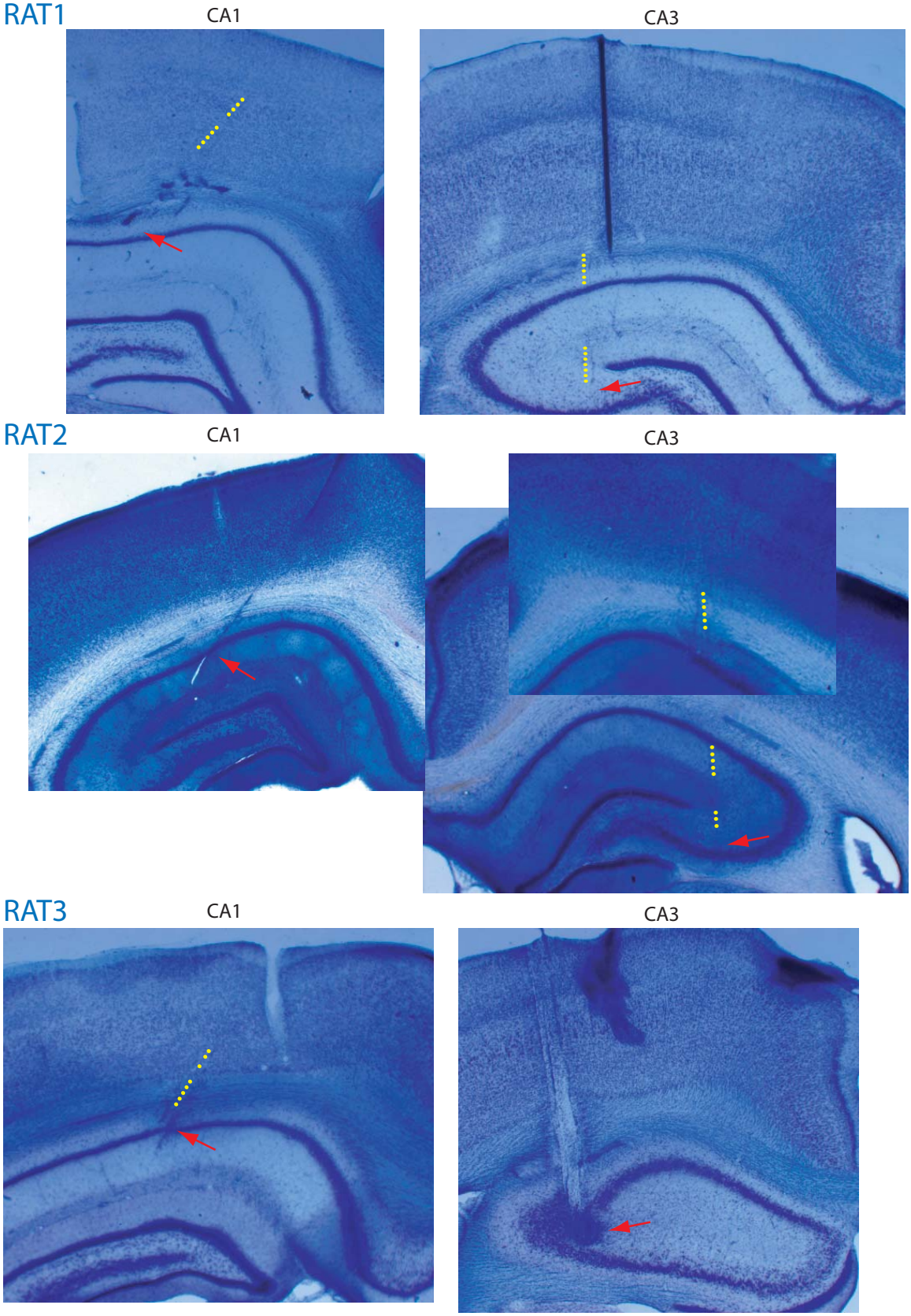

Nissl stained 100 µm thick brain slices confirm electrode locations. Lesioning was performed on Rat 3, with 4 µA current injected into the recording electrodes for 10 seconds. The minimal tissue damage caused by silicon microprobes makes visual identification of the electrode locations more difficult. Yellow dotted lines are interpolations based on adjacent sections, such as shown for Rat 2. CA3 electrodes were inserted vertically in the left hemisphere of anterior (dorsal) hippocampus (~2.8 mm posterior to bregma and ~2.6 mm lateral to the midline). CA1 electrodes were more posterior (~4.5 mm to bregma, and ~2.3 mm lateral to the midline) and inserted at an angle (25-35^0). Additionally, the CA1 pyramidal layer was identified electrophysiologically by the presence of sharp-wave ripple events in the local field. For CA3, electrodes were advanced beyond the CA1 pyramidal layer until a high-density of units was recognized.

Supplementary Figure S2

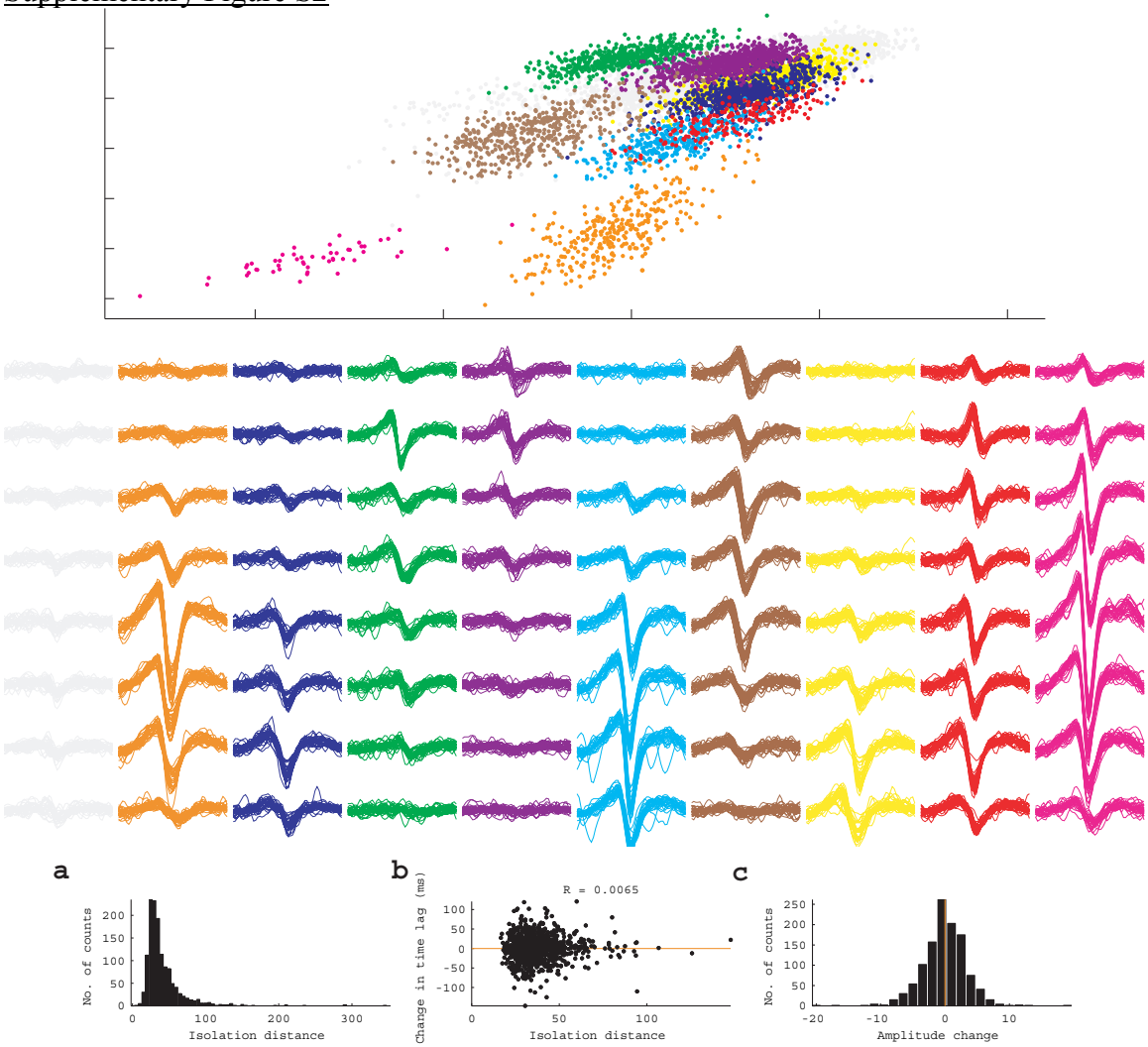

Cluster recorded from a single shank during a sample session are plotted. The top panel shows the projection on two principal component axes for noise (grey) and nine other clusters. Sample waveforms from all 8 electrode positions are shown in the middle panel. The lower panel depicts, from left to right: **a**) a histogram of the isolation distance

calculated along 24 feature components of all clustered cells(Harris et al., 2000; Schmitzer-Torbert et al., 2005). The median isolation distance was 33.8. **b**) The isolation distance was uncorrelated with the change in time lag from the long to the short track. **c**) Recordings were stable: the inset is a histogram of the percentage change in the mean spike amplitude for all recorded clusters (across all sessions), calculated from the electrode demonstrating the largest amplitude, for each recorded unit, from the long to the short track. The mean change was 0 ± 3 %, with no systematic drift.

Supplementary Figure S3

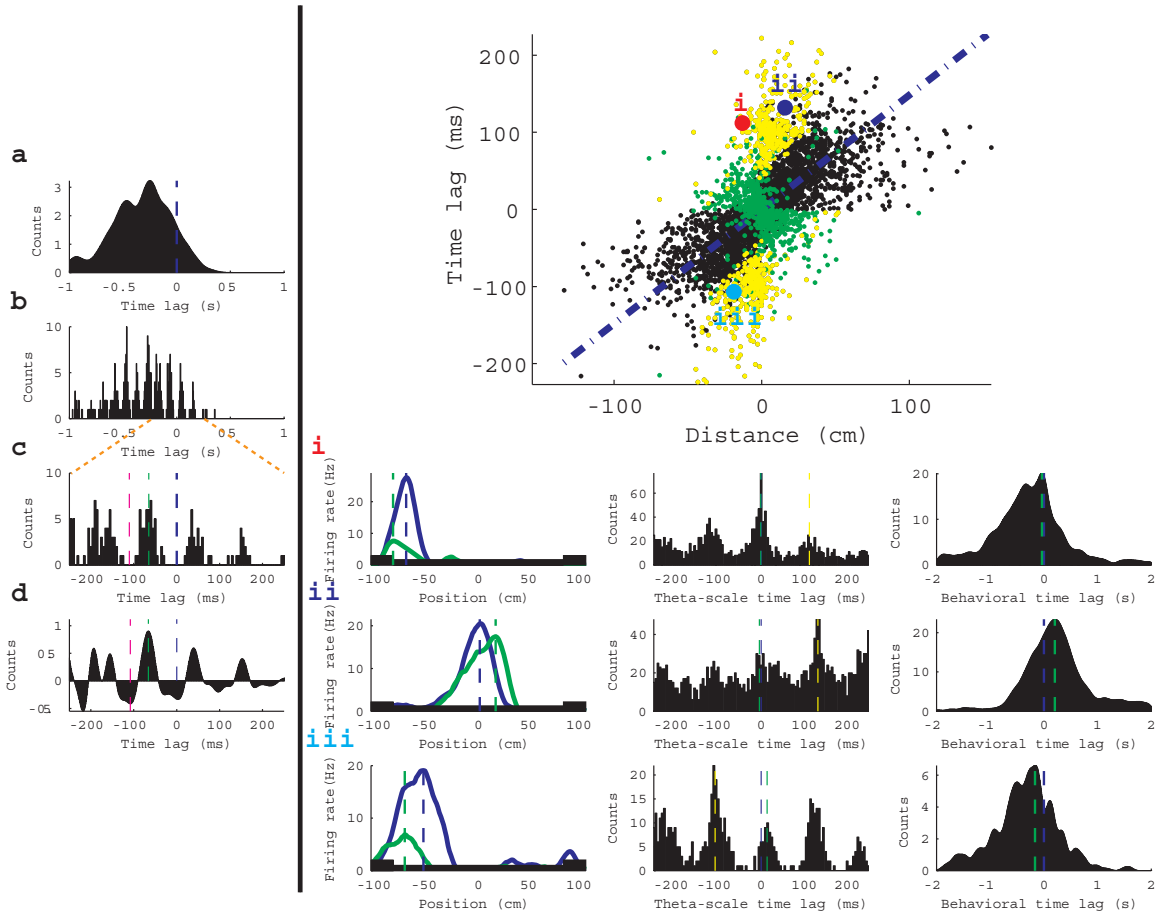

The left panel indicates the method for calculating the time lags. From top to bottom, **a**) first the direction of peak in the low-pass filtered CCG, on the behavioral timescale, was identified (here negative), relative to zero lag (**blue**). **b**) The unfiltered CCG (5 ms bins) is shown next. **c**) Zooming into the theta timescale, we identified the first peak (**green**) and the neared minima (**magenta**) in the **d**) band-pass filtered CCG (1ms binned). The corresponding values in the unfiltered (5 ms binned) CCG were recorded and used to evaluate if the peaks and valleys were sufficiently large (see methods). Step (a) in this algorithm occasionally misappropriates the direction of the time lag, necessitating error correction. The right panel illustrates the error-correction algorithm. We calculated the best-fit line (**dashed blue**) for sequence compression (top panel). If the time lag in the alternate direction (**green**), is closer to the best-fit line, we swap the original time lag (**yellow**), for this time lag. Three examples of swapping, (**i**), (**ii**), and (**iii**), are illustrated.

From left to right, panels show the place-fields, the CCG on the theta timescale, and the CCG on the behavioral timescale. The original and swapped time lags are indicated in the middle panel.

Supplementary Figure S4

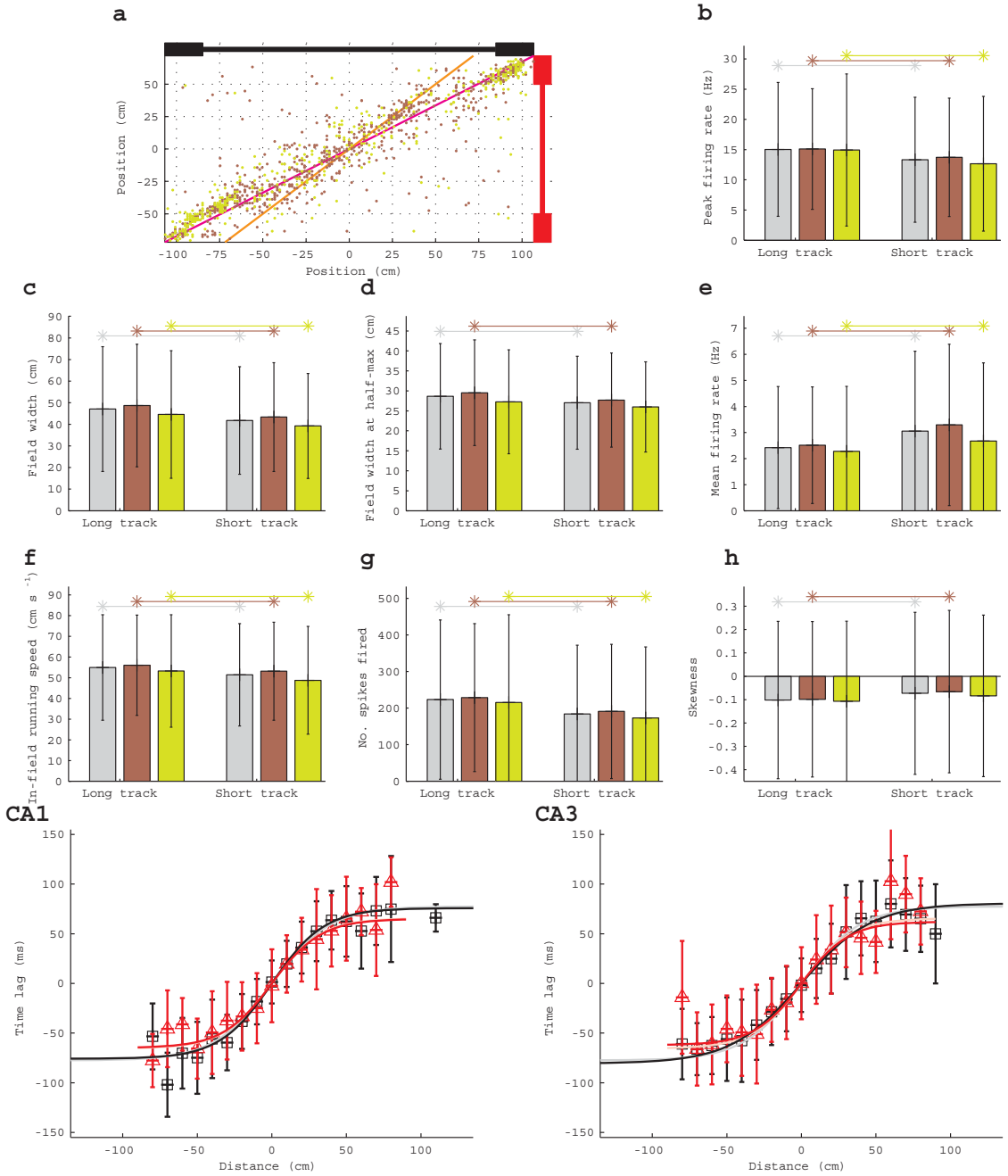

No clear systematic differences could be discerned from the place cell properties of CA1 (**brown**) or CA3 (**yellow-green**) vs. all cells combined (**grey**). Significant changes ($p < 0.05$) are indicated with an asterisk using rank-sum or t-tests, depending on the underlying distribution. From left to right, top to bottom, the panels depict the following: **a**) the preferred firing locations of cells on the long and shot tracks. **b**) The peak firing rates were lower on the short track. For field-width, defined as the length of the track for

which the cell fired ≥ 2 Hz (**c**) or defined as the width at half-maximum firing rate (**d**), significant decreases were observed. **e**) The mean firing rates increased from the long to the short track. This may have been due to the shorter amount of time rats spent on the short track. **e**) The in-field running speed (calculated by taking the average instantaneous speed of all spikes fired within the field) changed between environments. **g**) As expected, a greater number of spikes were fired on the long vs. the short track. **h**) Fields were more symmetric on the short track. The same sequence compression was observed for CA1 and CA3. Lower panels shows the sigmoidal sequence compression relationship on the long (**black**) and short (**red**) tracks. The sequence compression relationship for pooled CA1 and CA3 cell-pairs, from Figure 3 (main text), is also shown in faded colors. No difference is discernable.

Supplementary Figure S5

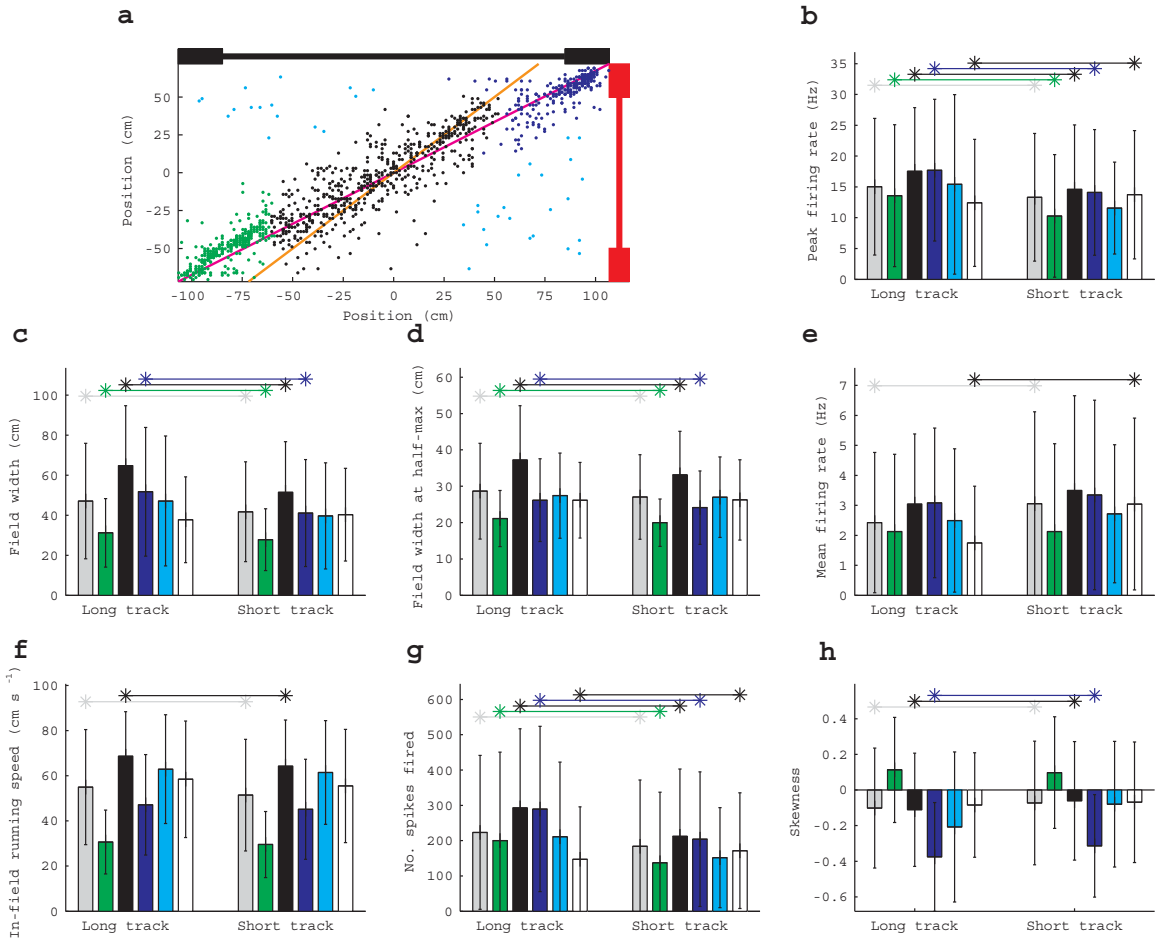

Place cell properties for each of the cell groups from Figure 1e (panel (**a**) here) are depicted for both track lengths. Place-fields at the beginning of the track tended to shift out towards the center (**green**), those in the middle did not shift or barely shifted (**black**), and those at the end of the track shifted in towards the center (**blue**), while a small fraction of fields re-mapped (**cyan**). Grey indicates all cells which fired on the track in each configuration, and white indicates cells that fired only in one configuration. Significant changes ($p < .05$) are indicated with an asterisk using rank-sum or t-tests, depending on the underlying distribution. From left to right, top to bottom, the panels

depict the following: **b**) The peak firing rates were significantly lower for all cells except for those that remap. For field-width, defined as the length of the track for which the cell fired ≥ 2 Hz (**c**) or defined as the width at half-maximum firing rate (**d**), significant decreases were observed for the same groups as in (**b**) minus those that fired on only one of the tracks. **e**) The mean firing rates increased from the long to the short track, most significantly in the subset that fired only on one track. This may have been due to the shorter amount of time rats spent on the short track **e**) Despite the general speed profile (**Figure 2d**), the in-field firing rates (calculated by taking the average instantaneous speed of all spikes fired within the field) changed between environments, mostly in the subset at the center. **g**) As expected, a greater number of spikes were fired on the long vs. the short track. **h**) The skewness of the fields was location dependent, with cells near the platform ends tailing towards the middle of the track. On the short track, place fields were less skewed.

Supplementary Figure S6

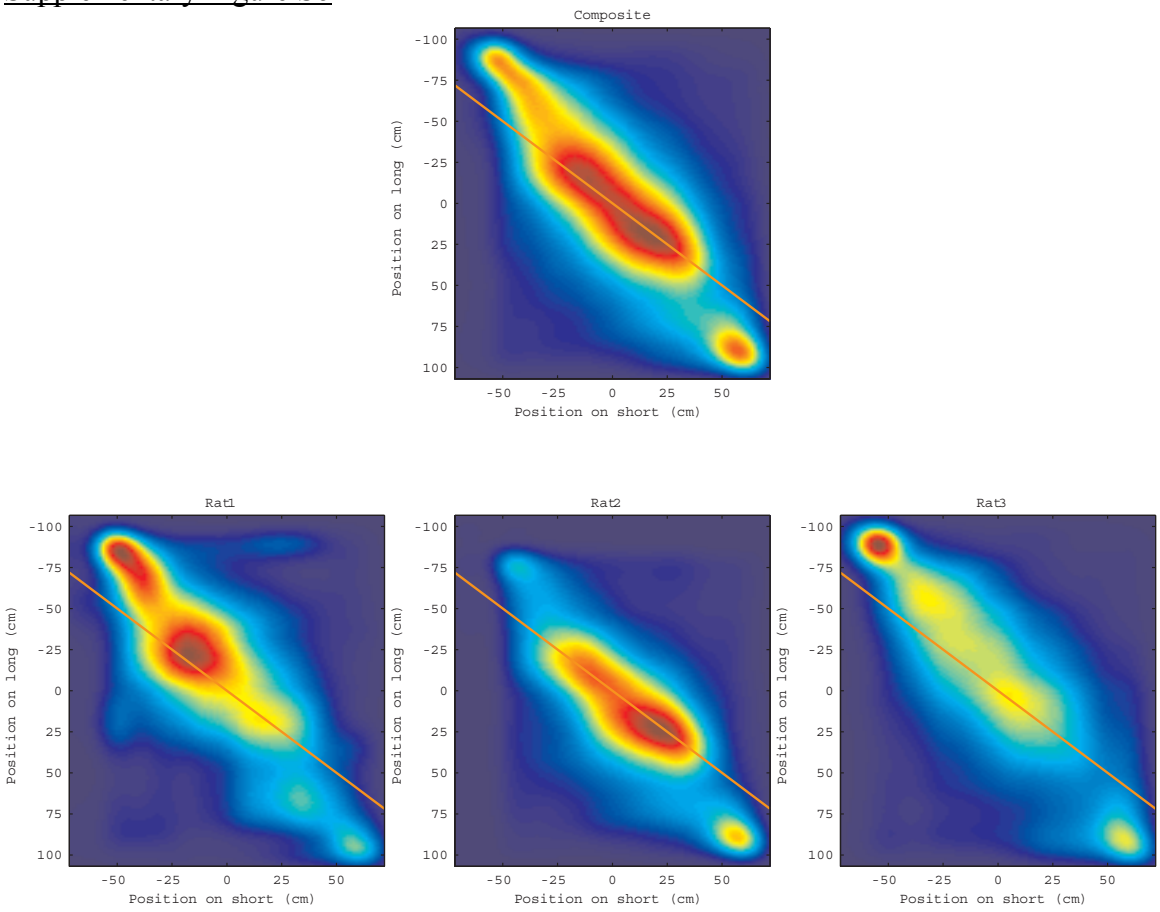

We calculated the populations vectors (Gothard et al., 1996) on the long and short tracks using the (smoothed) firing rates of every neuron at each distance bin. The cross-correlation of the population vectors between the long and short tracks supports the argument that the hippocampus switches references frames twice as the ran runs in direction of increasing (positive) position; the first switch occurs shortly after the rat leaves the start platform, and the second switch happens before he enters the end platform. The identity (no change) line is indicated in **orange**.

Supplementary Figure S7

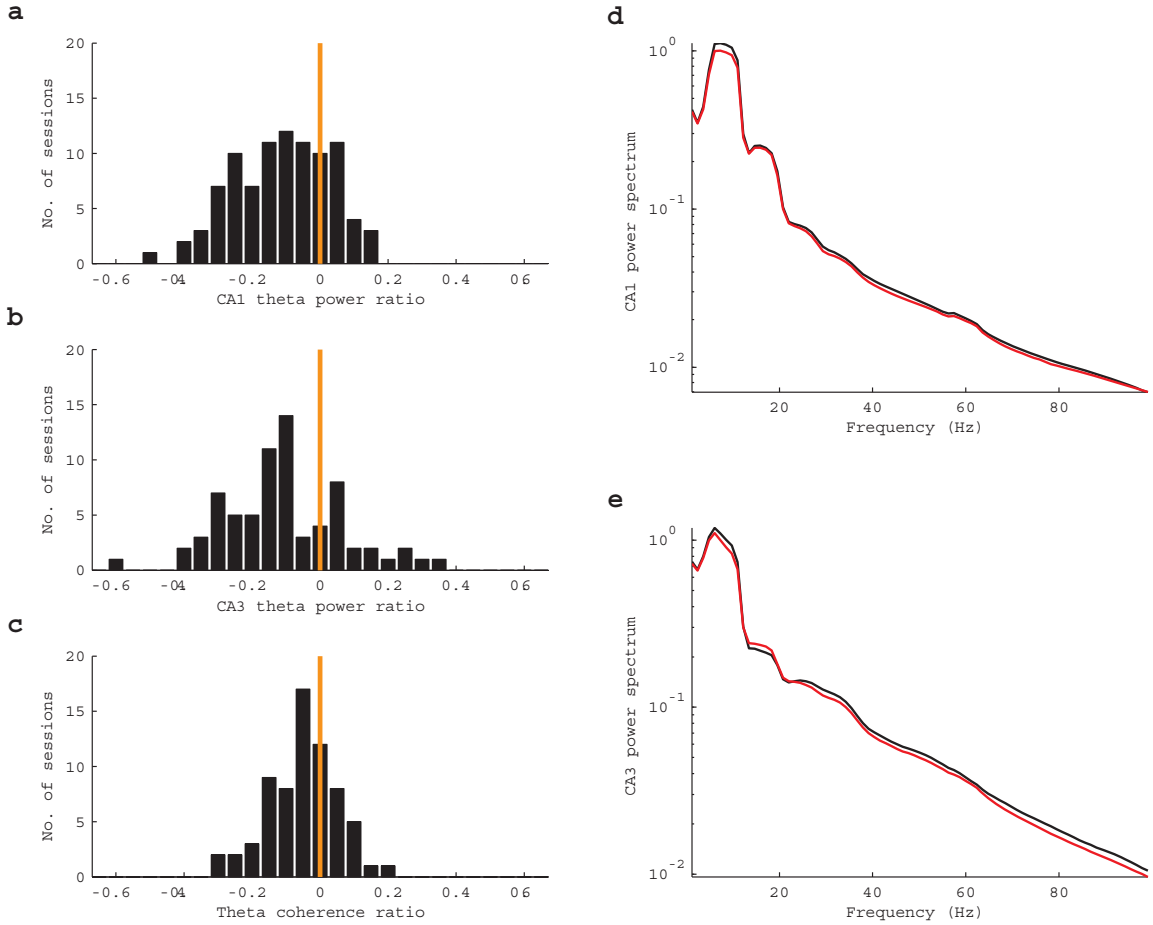

The theta power, compared across all sessions, was 10 % lower in **a**) CA1 (top; paired t-test $p < 10^{-10}$) and 9 % lower in **b**) CA3 (middle; paired t-test $p < .00005$) on the short track relative the long track. **c**) The theta-frequency band coherence also showed a small decrease (4.5 %; paired t-test $p < .0004$), from the long to the short track. The **orange** line indicates no change. The power spectrum in **d**) CA1 and **e**) CA3, normalized relative to the theta-band peak, and averaged across all sessions, showed a decrease in the theta band, as well as frequencies > 20 Hz, on the shortened track.

Supplementary Figure S8

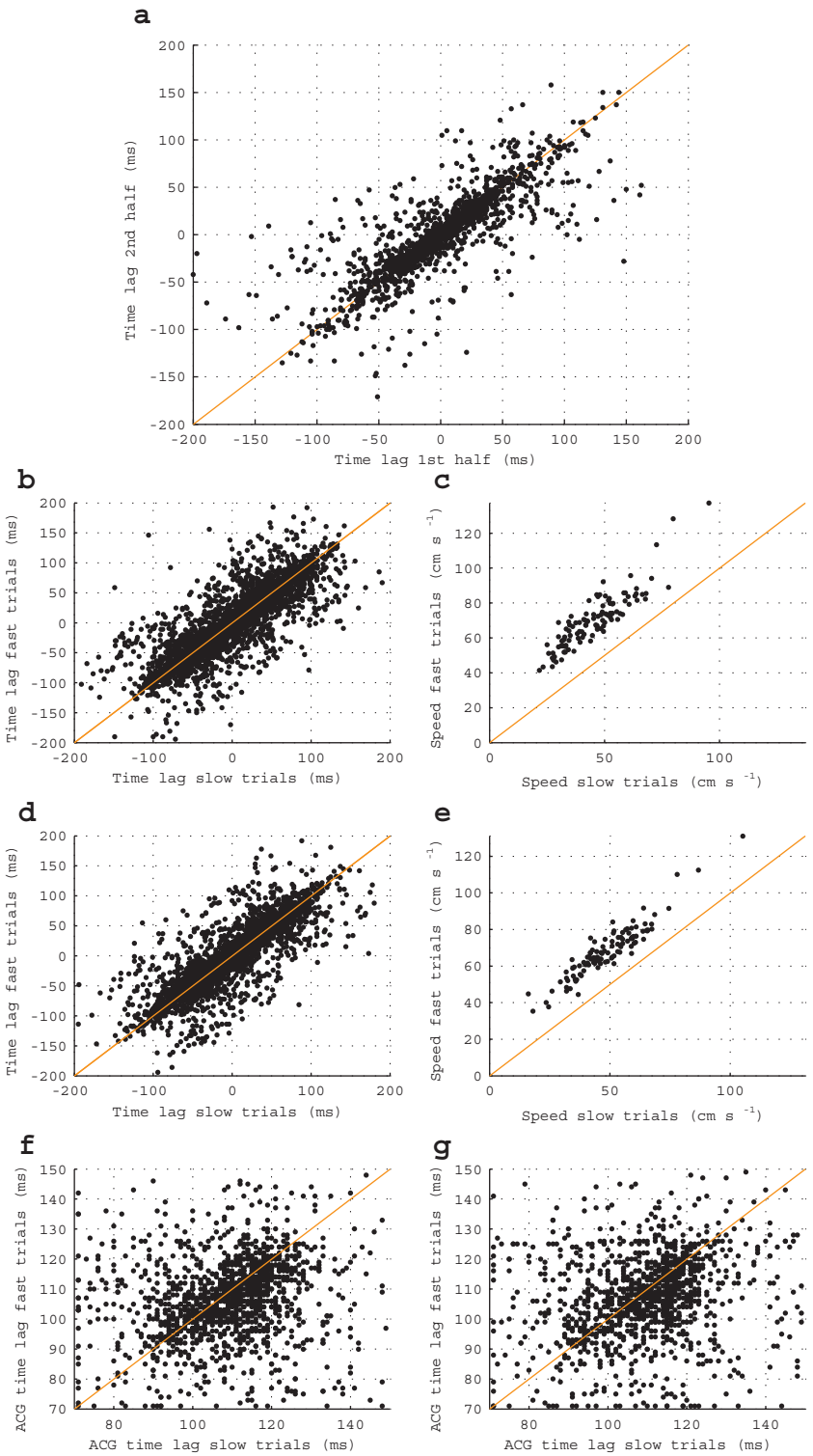

a) The time lag did not change from the first half to the second half of the trials on the short track, suggesting that the time-course of plasticity is longer than that of one session. The **orange** line indicates the identity. **b-g**)We split trials (laps) according to the running speed, and calculated the time lags separately on the slowest half (mean speed = 45.5

cm/s long; 48.6 cm/s short) and the fastest half (mean speed = 70.2 cm/s long; 67.9 cm/s short) of trials. The time lag was not affected by running speed on either (**b**) the long or (**d**) the short track, though the average running speeds of the speed-separated trials were indeed substantially different on both the (**c**) long and (**e**) short tracks. The **orange** line indicates the identity. In contrast, the time lags in the auto-correlograms, which indicate the oscillation frequencies of the cells, were significantly larger (slower) on the slow trials relative to the fast trials on both (**f**) the long track (t-test $p< 10^{-6}$) and (**g**) the short track (t-test $p< 10^{-3}$), consistent with the change in oscillation frequency (Geisler et al., 2007).

References for Supplementary Materials

Geisler C, Robbe D, Zugaro M, Sirota A, Buzsaki G (2007) Hippocampal place cell assemblies are speed-controlled oscillators. Proc Natl Acad Sci U S A 104:8149-8154.

Gothard KM, Skaggs WE, McNaughton BL (1996) Dynamics of mismatch correction in the hippocampal ensemble code for space: interaction between path integration and environmental cues. J Neurosci 16:8027-8040.

Harris KD, Henze DA, Csicsvari J, Hirase H, Buzsaki G (2000) Accuracy of tetrode spike separation as determined by simultaneous intracellular and extracellular measurements. J Neurophysiol 84:401-414.

Schmitzer-Torbert N, Jackson J, Henze D, Harris K, Redish AD (2005) Quantitative measures of cluster quality for use in extracellular recordings. Neuroscience 131:1-11.